IEEE Access
Multidisciplinary ⋮ Rapid Review ⋮ Open Access Journal

Received 22 November 2023, accepted 9 December 2023, date of publication 18 December 2023,
date of current version 27 December 2023.

Digital Object Identifier 10.1109/ACCESS.2023.3344394

THEORY

On the Sideband Harmonics in Pulsed Frequency Diverse Arrays

IHSAN KANBAZ[1,2], (Member, IEEE), UGUR YESILYURT[3], (Member, IEEE), GALIP ORKUN ARICAN[2], (Member, IEEE), ERTUGRUL AKSOY[2], (Member, IEEE), AND MICHAIL MATTHAIOU[1], (Fellow, IEEE)

[1]Centre for Wireless Innovation (CWI), Queen's University Belfast, BT3 9DT Belfast, U.K.
[2]Department of Electrical and Electronics Engineering, Gazi University, 06560 Ankara, Turkey
[3]Electrical and Electronics Engineering Department, Erzurum Technical University, 25050 Erzurum, Turkey

Corresponding author: Ihsan Kanbaz (ihsankanbaz@gazi.edu.tr)

This work was supported by the European Research Council (ERC) under the European Union's Horizon 2020 Research and Innovation Programme under Grant 101001331.

ABSTRACT Pulsed frequency diverse arrays (FDAs) have recently garnered significant research attention in radar and sensing applications due to their range-dependent radiation properties. However, the time-dependent nature of radiation can limit the benefits of FDAs. While recent methods have been proposed to mitigate this limitation and enhance the functionality of FDAs, there is an urgent need to better characterize their radiated power profile and specifically to address the substantial power losses in the sideband harmonics. In this paper, we bridge this gap in the literature by presenting a new closed-form expression for the sideband radiated power (SRP). Additionally, we explore practical limitations outlined in the existing literature that pertain to achieving time-independent radiation concerning SRP consumption. Finally, our theoretical analysis is supported by numerical examples. A noteworthy insight from our work is that treating pulsed FDA systems as time-independent may lead to unreliable conclusions, underscoring the importance of addressing the SRP issue in future research.

INDEX TERMS Frequency diverse arrays, harmonic analysis, radiated power, range dependent electric field.

I. INTRODUCTION

In point-to-point communication systems, spatial filtering is an inherently important process in increasing the quality of the channel. In this context, there is a common view that filtering must start from the antenna unit to achieve the desired signal-to-noise ratio (SNR) level. Spatial filtering in traditional array antenna systems is only accomplished in the angular domain, but with frequency diverse array (FDA) systems, it is also possible to filter in the range domain in addition to the angular domain [1], [2]. Interestingly, FDAs have recently found applications in radar [3], sensing [4] and eavesdroppers/clutter suppression [5], [6] scenarios.

In its most basic form, an FDA seeks to transmit an information signal modulated at different periods through its array elements [7]. This linear system achieves maximum radiation in the common period of all elements. Hence, for an electromagnetic wave traveling at the speed of light, a range-dependent radiation characteristic is obtained in a fixed time [8]. It is thought that this range-dependent radiation could be an innovative solution to the difficulties already being studied, such as clutter suppression, anti-jamming, and beam focusing [9], [10], [11]. Against this background, many types of FDAs that can be integrated with different application scenarios, have been introduced in the literature [12], [13], [14], [15]. Early studies have concentrated on beam focusing to transfer more power to the receiver in a desired area but neglected the influence of time dependency [16]. Thus, unlike classical phased antenna arrays (PAAs), FDAs are intimately designed to eliminate the range and angle coupling for beam steering. For this purpose, studies using nonlinear, multi-carrier, and

The associate editor coordinating the review of this manuscript and approving it for publication was Weiren Zhu.

optimized frequency increments among the elements have been conducted over the past years [17], [18], [19]. However, when electromagnetic wave propagation phenomena are examined, it is understood that these studies can focus the radiation only on the targeted position in a certain period of time and divert the radiation to a different position at other times [20]. As a result, these studies cannot decouple the angle and range dependency, which inevitably complicates beam-steering, particularly for communication and radar applications, due to the illumination of the target for a short time [21]. To overcome these fundamental limitations, time-independent as well as range-dependent radiation has gained attention [22], [23], [24]. First, it has been proposed that a time-independent radiation pattern can be obtained using time-dependent frequency offsets [25]. However, this approach faces some critical challenges. The first is that maximum radiation occurs only at the targeted location while remaining time-dependent at other angles and range values. Therefore, it would not be an appropriate approach to call these methods time-independent [26]. Another issue is that the phase and frequency relationship is not taken into account. The phase of a signal is calculated by integrating the frequency over a period of time. In other words, if the frequency increment is time-dependent, the signal phase cannot be written directly as a function of the frequency [27]. Surprisingly, these issues have been overlooked in papers focusing on time-invariant radiation. Although some studies have focused on the frequency and phase relationship to rectify the existing misconceptions, the results are time-dependent and far from beam-focused requirements [28].

Another approach aimed towards time-independent radiation is the concept of pulsed FDAs [29]. In this configuration, the input signals of varying frequencies are multiplied by a rectangular wave of predetermined duration before being transferred to the antenna elements. Under the criterion of choosing the pulse duration small enough, it has been suggested that the total radiation is quasi-static. Although this method does not completely remove the effect of time on the pattern, it does have a mitigating effect [28]. We point out that most studies on pulsed FDAs in the literature have investigated the time-domain behavior of radiation. Nevertheless, due to periodic switching, the frequency spectrum inherently contains infinite harmonic components, and, hence, a frequency domain analysis is indispensable to characterize rigorously the system's radiation profile [30].

To the best of the authors' knowledge, however, very limited studies have looked into the harmonic analysis of pulsed FDAs [30], [31]; there are no studies deriving a closed-form expression of the harmonic radiated power of pulsed FDAs. The main contributions of this paper are the following:

- We pursue a frequency-based analysis that facilitates a comprehensive understanding of the radiation properties specific to pulsed FDA systems.

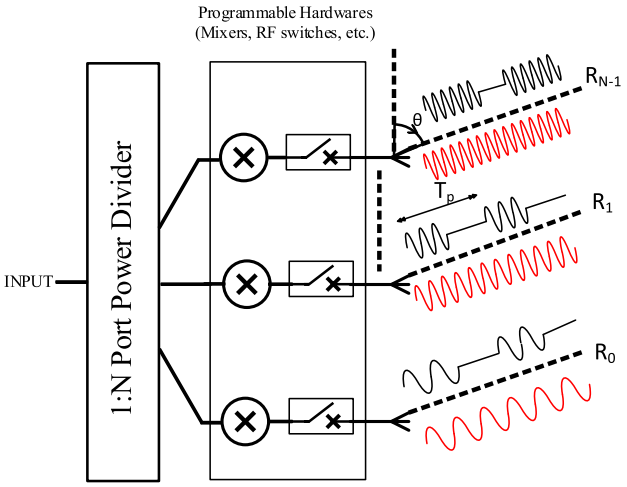

FIGURE 1. The geometry and waveform of an FDA: The red line represents a conventional FDA, while the black line represents a pulsed FDA.

- Recognizing the harmonic-based and range-dependent radiation properties experienced by each harmonic, we deduce an analytical expression of the power consumed at the harmonics of pulsed FDA systems.
- Using this expression, which we verify numerically, we conclude that the constraints previously proposed in the literature to achieve time-independent radiation impractically increase the power consumed at harmonics and, thus, are unsuitable for range-dependent and time-independent applications.

The rest of the paper is organized as follows: In Section II, the background of FDAs with special emphasis on conventional and pulsed FDAs is given. In Section III, the frequency analysis of pulsed FDAs is performed by using a Fourier series representation. Section IV analyzes the power loss caused by periodic switching and derives a closed-form expression for the SRP. Section V provides numerically validated examples, findings, and discussions. Finally, Section VI concludes the paper.

II. BACKGROUND OF FDAS

The physical construction and mathematical foundations of FDA-based systems are described in detail in this section. We first focus our attention on basic FDA systems, followed by a brief report on the time domain analysis of pulsed FDA systems, which is one of the strategies to achieve time-independent radiation that has already been adopted in some recent works [29], [30], [32].

A. CONVENTIONAL FDAS

Although an FDA has the same physical layout as standard array antennas, it is distinguished from others by the frequency shifting front-end devices used in antenna terminals. In other words, and as shown by the red lines in Fig. 1, each antenna element transmits the same information signal at different frequencies. The signal transmitted by the n-th

isotropic antenna element is written as follows:

$$S_n(t) = \alpha_n e^{j2\pi f_n t}, \quad n = 0, 1, \ldots, N-1, \tag{1}$$

where α_n and f_n represent the input signal's amplitude weighting and frequency, respectively. Due to the array's linearity, the total electric field at the far-field emitted by the N element array is calculated by the sum of the electric fields emitted by each element and expressed as follows:

$$s(t) = \sum_{n=0}^{N-1} \alpha_n e^{j2\pi f_n \left(t - \frac{R_n}{c}\right)}, \tag{2}$$

where c and R_n denote the speed of light and the distance of the array element from the observation point, respectively. If the excitation frequencies are chosen to be in the Δ_{f_n} vicinity of a specific frequency (i.e., $f_n = f_0 + \Delta_{f_n}, n = 0, 1 \ldots N-1$) and $R_n \approx R - nd\cos\theta$ under the far-field approximation (i.e. R_n is much greater than Rayleigh distance), the total electric field for a N element linear array located at z axis can be written as follows [10]:

$$s(t, R, \theta) = e^{j2\pi f_0 (t - \frac{R}{c})} \sum_{n=0}^{N-1} \alpha_n e^{j2\pi f_0 nd\cos\theta/c} \times e^{j2\pi \left(\Delta_{f_n}\left(t - \frac{R}{c}\right) + \frac{\Delta_{f_n} nd\cos\theta}{c}\right)}, \tag{3}$$

where d represents the Euclidean distance between the array elements, and θ represents the observation angle at the far-field. The total electric field, as shown in (3), is affected by t, Δ_{f_n}, and R in addition to the phased array system parameter θ. Hereby, it has been proposed that with appropriate Δ_{f_n}'s, a range-dependent pattern can be generated. Note that (3) is a general electric field expression for an FDA. When the frequency difference between the elements is given by a linear equation (i.e $\Delta_{f_n} = n\Delta_f$), the array factor of the system can be written as follows [33]:

$$AF(t, R, \theta) = \sum_{n=0}^{N-1} e^{j2\pi n\left(f_0 d\cos\theta/c + \Delta_f\left(t - \frac{R}{c}\right) + \frac{\Delta_f n^2 d\cos\theta}{c}\right)}. \tag{4}$$

Here, the quadratic term $\frac{\Delta_f n^2 d\cos\theta}{c}$ can be ignored whenever $\Delta_f \ll f_0$. Hence, (4) can be rewritten as follows [34]:

$$AF(t, R, \theta) = \sum_{n=0}^{N-1} e^{jn2\pi\left(f_0 d\cos\theta/c + \Delta_f\left(t - \frac{R}{c}\right)\right)}. \tag{5}$$

In its final form, (5) incorporates time, range, and angle-dependent radiation characteristics. The radiation's angle dependency is well known from the field of phased array systems. However, the dependence of radiation on the range is a relatively new phenomenon. Nevertheless, it is thought that it may be a viable solution to existing problems in applications such as radar, jammer blocking, secure communication, and wireless power transfer (WPT) [31], [35], [36].

As seen in Fig. 1, periodic signals are applied to the input of the antenna elements. The sum of these periodic signals, with extremely small frequency differences, is also periodic, and the range dependency is caused by the periodicity of the sum of these signals. As a result, in the common period of all elements, the total radiation becomes maximum/minimum. Since the electromagnetic wave travels in time at the speed of light, If time is periodic, there is also periodicity in the range domain. By observing that the time and range periodicity stems from (5), which includes exponential terms, thus, the system is predicted to be periodic around 2π, so the time periodicity can be defined as follows [37]:

$$\gamma_{t+t_p} = \gamma_t + 2\pi, t_p = \frac{1}{\Delta_f}, \tag{6}$$

while the range periodicity is defined as follows:

$$\gamma_{R+R_p} = \gamma_R + 2\pi, R_p = \frac{c}{\Delta_f}. \tag{7}$$

B. PULSED FDAS

Although it brings a brand-new research area to the antenna and propagation community, it is thought that the time periodicity in classical FDAs overshadows the benefits of the range-dependent radiation pattern. As a result, studies have been conducted to address the disadvantages of the time parameter while aiming at pure range-dependent characteristics. One of the most promising architectures is a pulsed FDA system [29]. As shown by the black lines in Fig. 1, unlike the classical FDA, the input signal applied to the antennas is multiplied by a square wave with a certain period and duration. In other words, (1) is written by converting it as follows:

$$S_n^P(t) = \lceil \tau_n \rceil \alpha_n e^{j2\pi f_n t}, \quad n = 0, 1, \ldots, N-1, \tag{8}$$

where $\tau_n = t_n f_p$ and $\lceil . \rceil$ represents the normalized pulse duration of the square wave with $f_p = \frac{1}{T_p}$ frequency and rectangular function for certain duty cycle, respectively. Henceforth, the superscript 'P' represents the pulsed operation. Hence, (3) should be modified for uniform frequency spacing (i.e., $f_n = f_0 + n\Delta_f$) to obtain the pulsed FDA's field for the same pulse duration of array elements. In other words, the total electric field can be expressed in the following form

$$s^P(t, R, \theta) = e^{j2\pi f_0\left(t - \frac{R}{c}\right)} \lceil \tau_n \rceil \sum_{n=0}^{N-1} \alpha_n e^{jn\gamma}. \tag{9}$$

Here, we define $\gamma \triangleq 2\pi\left(\frac{f_0 d_n \cos\theta}{c} + \Delta_f\left(t - \frac{R}{c}\right)\right)$. Most importantly, the radiation of the pulsed FDA system is time, angle, and range dependent. However, some studies claim that by reconfiguring the structural parameters of pulsed FDAs, time-independent but range-dependent radiation can be obtained [29]. In these studies, it has been reported that the pulse length should be chosen rather small to neglect the time-induced phase delays. In other words, the maximum phase difference that may occur in the antenna array during the time the element is turned on, is intended to be negligible. Hence, the maximum phase difference is expressed as [29]:

$$\psi = (N-1)\left(\gamma|_{t=t_n} - \gamma|_{t=0}\right) = (N-1)2\pi\Delta_f t_n. \tag{10}$$

When $(N-1)\Delta_f t_n \ll 1$ is selected, the radiation becomes almost quasi-static. That is, the time expression in (9) is negligible. To achieve this, the condition $t_n \ll \frac{1}{\Delta_f}$ must be satisfied. With this approach, it is suggested that the radiation occurs entirely in range-angle couplings. However, customizing such radiation characteristics by ignoring the time parameter, is far from plausible [20].

III. FREQUENCY DOMAIN ANALYSIS

The existing pulsed FDA operation stems from modulating the classical FDA with a periodic sequence. To date, most studies in this space have not addressed a fundamental issue, that is that the periodic modulation causes the harmonics of the applied signal to spread in the frequency spectrum at the linear multiples of f_p. As an illustration, the distribution of harmonics for a 3-element pulsed FDA is shown in Fig. 2 for a better understanding of this phenomenon. More specifically, harmonics of the same order of the array elements are decomposed by Δ_f and are located in the frequency spectrum. The frequency at which harmonics of the same order begin to diverge is determined by the pulse repetition frequency (f_p), and this is repeated at each linear multiples of f_p. Therefore, a time-domain analysis is not sufficient to understand and characterize the radiation profile. Moreover, it is also crucial to consider the harmonic behavior due to periodicity like in time modulated arrays (TMAs) [38].

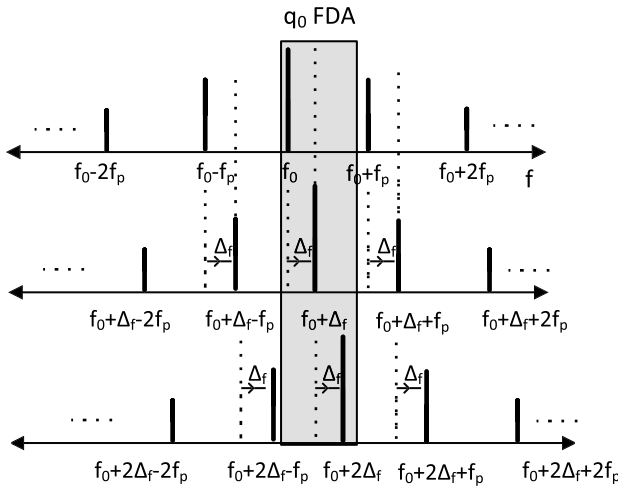

FIGURE 2. Representation of the pulsed FDA's harmonic coefficients' distribution.

In this regard, it is necessary to start with the Fourier series expansion of the rectangular function in (8). This is expressed as follows:

$$\lceil \tau_n \rceil = \sum_{q=-\infty}^{q=\infty} C_n^q e^{jqw_p t}, \tag{11}$$

where $w_p = 2\pi f_p$, C_n^q, $q \in \mathbb{Z}$, represent the pulse angular frequency, Fourier series coefficient and harmonic order, respectively. When (11) is plugged into (9), the field expression becomes [30]:

$$\begin{aligned} s^P(t,R,\theta) &= \sum_{q=-\infty}^{\infty} e^{j2\pi(f_0+qf_p)\left(t-\frac{R}{c}\right)} \\ &\times \sum_{n=0}^{N-1} \alpha_n C_n^q e^{j2\pi(f_0+qf_p)nd\cos\theta/c} e^{j2\pi n\left(\Delta_f\left(t-\frac{R}{c}\right)\right)}. \end{aligned} \tag{12}$$

The total radiation, as shown in (12), contains an infinite number of harmonic components. These are divided into two categories, namely the $q = 0$ component formed at the carrier's center frequency and the $q = \pm1, \pm2, \pm3, \ldots$ components formed in the remaining sidebands. If the on-time duration of the nth element is represented by t_n as $0 \le t \le t_n$, the C_n^q terms are obtained as follows [39]:

$$C_n^q = \begin{cases} \tau_n, & q = 0 \\ \dfrac{\sin(q\pi\tau_n)}{q\pi} e^{-jq\pi\tau_n}, & q \neq 0. \end{cases} \tag{13}$$

Hence, the array factor for $q = 0$ is obtained as

$$AF_0^P(t,R,\theta) = \sum_{n=0}^{N-1} \alpha_n \tau_n e^{j2\pi(f_0)nd\cos\theta/c} e^{j2\pi n\left(\Delta_f\left(t-\frac{R}{c}\right)\right)}, \tag{14}$$

while the array factors for sideband radiations are obtained as follows:

$$\begin{aligned} AF_q^P(t,R,\theta) &= \sum_{n=0}^{N-1} \alpha_n \frac{\sin(q\pi\tau_n)}{q\pi} e^{-jq\pi\tau_n} \\ &\times e^{j2\pi f_0 nd\cos\theta/c} e^{j2\pi n\left(\Delta_f\left(t-\frac{R}{c}\right)\right)}. \end{aligned} \tag{15}$$

In these expressions, the effect of the quadratic term is neglected by assuming that $\Delta_f \ll f_0$. It should be noted that if the $(N-1)\Delta_f < f_p$ constraint is satisfied, frequency differences between harmonics of the same order allow the entire system to be classified as harmonic order FDA (i.e. q_0 FDA, q_1 FDA, ...). Therefore, it can be conjectured that a range and time-dependent radiation occurs in each harmonic component.

IV. POWER LOSS CALCULATION

In this section, a power loss calculation over harmonics for pulsed FDAs is presented and a closed-form expression is derived by using known identities. To reduce the processing burden while not deviating from generality, a one-dimensional array of N isotropic antennas positioned on the z-axis is considered. Since the change of the geometric structure affects only the spatial integration, the solution presented for linear arrays can be easily extended to different geometries. In other words, the main processing burden comes from the calculation of the correlation between harmonics. Furthermore, to calculate the total radiated power, the average power density should be used as a starting point. By definition, the average power density is computed by integrating the square of the signal's amplitude across

a period. Furthermore, for electromagnetic waves it can be expressed as proportionate to the square of the real component [38], such that

$$\ddot{P}(\theta)_{avd} \propto \frac{1}{t_p}\int_{t_0}^{t_0+t_p} [\mathrm{Re}\langle s^P\rangle]^2\, dt. \tag{16}$$

Here, $\mathrm{Re}\langle\rangle$ represents the real part of the electric field, while $t_p = \frac{1}{\Delta_f}$ represents the periodicity of the pulsed FDA in the time domain. Moreover, the real part of (12) can be expressed as follows:

$$\mathrm{Re}\langle s^P\rangle = \sum_{q=-\infty}^{\infty}\sum_{n=0}^{N-1} |C_n^q| \cos(2\pi(f_0 + qf_p + n\Delta_f)t' + \varphi_{nq}). \tag{17}$$

In the above equation. $t' = (t - \frac{R}{c})$ and

$$\varphi_{nq} \triangleq \frac{2\pi(f_0 + qf_p)d_n cos(\theta)}{c} + \phi_{nq}, \tag{18}$$

where ϕ_{nq} represents the phase of the q-th harmonic of the n-th element. Due to the summation, $[\mathrm{Re}\langle s\rangle]^2$ should be analyzed in two parts: for $q = p$ and $q \neq p$ where q and p represent the integer harmonic orders. Hence, (17) for $q = p$ part is written as (19), shown at the bottom of the next page. Thus, the other part $q \neq p$ can be written as in (20), shown at the bottom of the next page. If (19) and (20) are substituted into (16), the average power density for $q = p$ turns out to be given by (21) below:

$$\underset{q=p}{\ddot{P}(\theta)_{avd}} = \sum_{q=-\infty}^{\infty}\frac{1}{t_p}\int_{t'=0}^{t_p}\sum_{n=0}^{N-1}|C_n^q|^2 \times \cos(2\pi(f_0 + qf_p + n\Delta_f)t' + \varphi_{nq})^2 dt'. \tag{21}$$

Under $T_p \gg T_0$, (21) can be simplified (a detailed proof is provided in the Appendix) according to

$$\underset{q=p}{\ddot{P}(\theta)_{avd}} = \frac{1}{2}\sum_{q=-\infty}^{\infty}\sum_{n=0}^{N-1}|C_n^q|^2. \tag{22}$$

Since the integral of the product of two cosine signals with different frequencies over a certain period equals zero, the case of $m \neq n$ is ignored (see Appendix). Therefore, we can consider only the $m = n$ and $q = p$ cases. After an integration using the spatial coordinates is applied (i.e. $0 \leq \theta \leq \pi$ and $0 \leq \phi \leq 2\pi$) [40], we obtain

$$P_h = \int_0^{2\pi}\int_0^{\pi} [\underset{\substack{q=p\\ q\neq 0}}{\ddot{P}(\theta)_{avd}}] \sin\theta d\theta d\phi. \tag{23}$$

Thus, the total radiated power at the harmonics is derived as follows [41]:

$$P_h = 2\pi\sum_{n=0}^{N-1}\tau_n(1-\tau_n). \tag{24}$$

Note that the power of the harmonics and main components are summed to determine the total radiated power including that of the $q = 0$ components, as follows:

$$P_T = P_0 + P_h. \tag{25}$$

When the same procedure is used to find P_0, (16) is evaluated for $q = 0$ as follows:

$$\underset{q=0}{\ddot{P}(\theta)_{avd}} = \frac{1}{t_p}\int_0^{t_p}\sum_{n=0}^{N-1}(\tau_n)^2\cos\left(2\pi(f_0 + n\Delta_f)\right)^2 dt. \tag{26}$$

Finally, when spatial integration is applied, the power of the $q = 0$ component is calculated as follows:

$$P_0 = 2\pi\sum_{n=0}^{N-1}(\tau_n)^2. \tag{27}$$

V. HARMONICS CHARACTERISTICS AND NUMERICAL VALIDATION

This section presents the comprehensive analysis of the effects of (24) and (15) on pattern synthesis and power consumption through comparative examples. Firstly, we discuss the extra design parameter introduced in (15) and its potential contribution to pattern synthesis. Secondly, we exemplify the impact of harmonic power consumption on the overall system performance through comparative examples using (24). Moreover, we compare the proposed expression with a numerical integration method to showcase its hardware/time consumption advantages. Finally, we briefly discuss the difficulties in obtaining the experimental verification of the results and state-of-the-art differences between the existing literature studies to better understand the pulsed FDA's benefits.

A. DISCUSSION ON PATTERN SYNTHESIS

It is inferred from the previous analysis that the pulsed FDA contains an infinite number of classic FDAs decomposed at linear multiples of the f_p frequency. In this case, as can be seen in (15) as well, the harmonic coefficients appear in the beampattern as an additional degree of freedom. Thus, by optimizing the switching function parameters (especially the normalized pulse durations τ_n), low sidelobe levels (SLL) can be achieved without using complex hardware in a cost-effective way. On the other hand, while switching is an effective technique for SLL reduction, it inherently suffers from sideband radiations. As a result, in several papers, SRP is evaluated as a power loss, while various optimization algorithms have been developed to suppress the undesired sideband radiations (see for instance [30], [39], [42]).

To demonstrate the aforementioned abilities of this technique in terms of pattern synthesis, we consider an example with $N = 20$, $f_0 = 10$ GHz, $\Delta_f = 350$ Hz, and $d = 0.5\lambda$, where λ represents the wavelength at the f_0 frequency (hereinafter referred to as Example-1). In this example, the pulse repetition frequency and on-time durations of all elements have been chosen equally to comply with the

form in which pulsed FDA was first introduced. Due to the same on-time durations, the harmonic coefficients of all elements in the same harmonic order are the same. Therefore, radiations in different harmonics differ from each other only in amplitude. As a result, the range characteristic of FDAs formed at each harmonic order is the same, differing only in amplitude (i.e., the $q_{0,1,2...}$ FDAs have the same range-angle pattern). It should be noted that the $f_p \ll f_0$ constraint must be preserved. Hence, the difference in this amplitude level is defined by the ratio of the harmonic coefficients of the elements in any harmonic order (i.e. $C_n^{q_{d1}}/C_n^{q_{d2}}$, where q_{d1} and q_{d2} denotes desired harmonic orders). If the pulse repetition frequency is selected as 1 MHz and the normalized on-time duration is chosen 0.4 for all elements, the range-angle radiation pattern is shown in Fig. 3a, while the amplitude ratio between the $q = 0$ and $q = 1$ radiations is -2.42 dB.

As an another example, the change of harmonic radiation patterns and power consumption values of pulsed FDAs, which consist of elements with different on-time durations, different from the general structure, will be examined (hereinafter referred to as Example-2). In particular, Figs. 4b–4d depict the angle-range patterns of the radiation that will occur at the $q = 0, 1, 2$ harmonics for $t = \frac{1}{\Delta_f}$. When the open times are adjusted to the Chebyshev coefficients of -20 dB (more specifically, $\tau_n = [0.58, 0.66, 0.88, 1, 1, 0.88, 0.66, 0.58]$), a notable distinction arises from the durations of previously demonstrated Example-1. As a consequence, the radiation levels will exhibit a continuous alteration within the angle-range couplings for every harmonic. The maximum radiation amplitude ratio of $q = 0$ and $q = 1$ harmonics is calculated to be approximately -14.79 dB. As can be seen from Example-1 and Example-2, choosing the same durations causes the sideband level to be quite high: -2.42 dB for the same duration case (Example-1), and -14.79 dB for the element-specific duration (Example-2) at specific range 200 km (see Fig. 3). Hence, this choice makes the signal be transmitted at high power levels over multiple frequencies. Additionally, this will compromise the frequency spectrum allocation and quality of secure communication.

The above considered examples are now evaluated in terms of SLL; in Example-1, the level of the SLL is approximately -13.2 dB, while it is calculated as -20 dB in Example-2. This allows the suppression of transmitter/receiver and signal/scattering sources located at undesirable angles. As a result, the system's radiation performance improves, and the first step toward establishing a secure communication environment is taken. In addition, it can be inferred from these two examples that the SLL and SRP levels can be reduced by carefully selecting the time durations.

Another crucial point concerning pattern synthesis is that most works on pulsed FDAs to date have focused on monochromatic signals. Although this simplifies the calculations, the input signal's bandwidth (B_w) is an important parameter to consider during system design. In this case, the bandwidth must be constrained to allow the system to function properly. If Fig. 2 is reviewed again in this context, it can be stated that there are two basic criteria for a bandlimited signal not to be distorted in the frequency spectrum. These are as follows:

1) $B_w < \Delta_f$; Thus, there will be no aliasing between the array's elements in the overall frequency response.
2) $(N-1)\Delta_f < f_p$: In order to avoid the distortion between consecutive harmonic orders. Otherwise, interference in the harmonics will kick in making it harder to reconstruct the signal.

B. DISCUSSION ON POWER CONSUMPTION

In this part, the consumption of the radiated power in pulsed FDAs is presented via comparative examples and validated with a numerical integration method. In these examples, the SRP value calculated by the derived equation presented in (24) and the numerical integration method has been examined to test the effectiveness of the closed-form

$$[\mathrm{Re}\langle s^P\rangle]^2 = \underbrace{\sum_{q=-\infty}^{\infty}\sum_{n=0}^{N-1}|C_n^q|^2\cos\left(2\pi(f_0+qf_p+n\Delta_f)\,t'+\varphi_{nq}\right)^2}_{m=n} + \underbrace{\sum_{q=-\infty}^{\infty}\sum_{n,m=0}^{N-1}|C_n^q||C_m^q|\cos\left(2\pi(f_0+qf_p+n\Delta_f)t'+\varphi_{nq}\right)\cos\left(2\pi(f_0+qf_p+m\Delta_f)t'+\varphi_{mq}\right)}_{m\neq n} \tag{19}$$

$$[\mathrm{Re}\langle s^P\rangle]^2 = \sum_{q=-\infty}^{\infty}\sum_{n=0}^{N-1}\underbrace{|C_n^q||C_n^p|\cos\left(2\pi(f_0+qf_p+n\Delta_f)t'+\varphi_{nq}\right)\cos\left(2\pi(f_0+pf_p+n\Delta_f)t'+\varphi_{np}\right)}_{m=n} + \sum_{q=-\infty}^{\infty}\sum_{n,m=0}^{N-1}\underbrace{|C_n^p||C_m^q|\cos\left(2\pi(f_0+qf_p+n\Delta_f)\,t'+\varphi_{nq}\right)\cos\left(2\pi(f_0+pf_p+m\Delta_f)t'+\varphi_{mp}\right)}_{m\neq n} \tag{20}$$

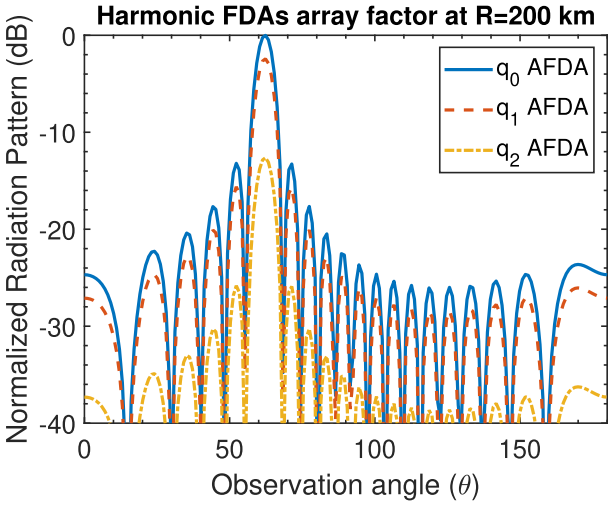

(a)

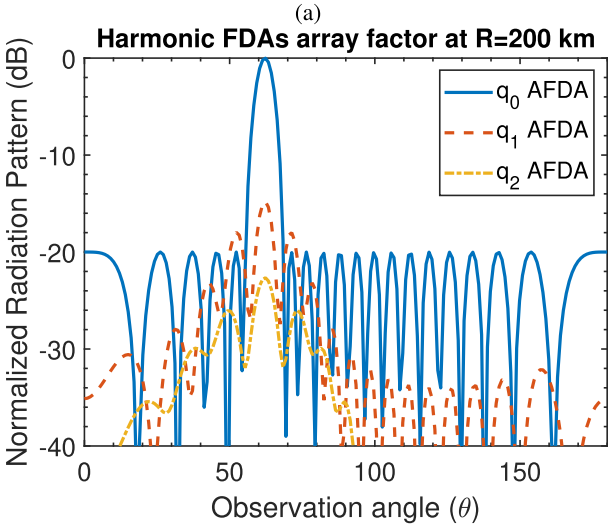

(b)

FIGURE 3. **(a) The normalized radiation pattern for identical pulse duration case (Example-1) in a fixed time ($t = 0.002857$ sec) and range (200 km) (see black dashed line in Fig. 4a); (b) The normalized radiation pattern for element-specific pulse duration (Example-2) for a fixed time and range (see black dashed line in Figs. 4b–4d).**

expression. For this purpose, the term $P_{loss}^{\%}$, which is the ratio of the SRP to the total power, is used as a benchmark tool to analyze the overall performance of the array. According to this definition, the term $P_{loss}^{\%}$ of the considered array is written as follows [41]:

$$P_{loss}^{\%} = \frac{P_h}{P_T} \times 100. \tag{28}$$

When Example-1 in Section V-A is investigated in terms of power consumption, the power loss is calculated as 60% using (24) and (28). This corroborates the fact that harmonics consume most of the radiated power. Apart from the observation that low on-time durations lead to a time-independent pattern (which has often been overlooked in the literature), there are associated disadvantages, like the increased power consumption in harmonics. For example, if the on-time duration is set to 0.01 as in [29], the belief that time-independent radiation can be obtained results in the consumption of 99% of the total power in harmonics. In other words, in addition to the studies in the literature on the disadvantages of this approach, impractical results are obtained in terms of power consumption as well. If we consider Example-2 in Section V-A (i.e. different on-time durations), the power consumption value is found to be 16.94%, which is quite low when compared to the previous example. This is a clear illustration of how $P_{loss}^{\%}$ can be reduced by changing the open time durations.

To test the effectiveness of the proposed closed-form expression, some array configurations [41], [42] and a 4-element pulsed FDA array (represented as [*] in the comparison table), whose parameters are given as $\Delta_f = 300$ KHz, $f_p = 20$ MHz, $\tau_n = [0.57, 1, 1, 0.57]$ are examined and discussed.

TABLE 1. **Comparison table between the proposed closed-form expression and trapezoidal numerical integration method.**

	Method	$P_{loss}^{\%}$	Elapsed time (seconds) ≈
[42]	(28)	16.18	0.0179
	Numerical	16.11	42980
[41]	(28)	18.52	0.0154
	Numerical	18.45	31882
[*]	(28)	15.48	0.0142
	Numerical	15.45	11676

The trapezoidal numerical integration method is used as the verification method. In this method, a truncated version of the pulsed FDA with infinite harmonics is used ($q_s = 100$). To put it more clearly, as can be understood from equation (13), the amplitudes of the harmonics are inversely proportional to the order. Therefore, the contribution of higher-order harmonics is too small and can be neglected (only the contribution of the $|q_s| < 100$ order harmonics to the power consumption is taken into account). Our numerical evaluations are implemented on a PC equipped with an i7 6700HQ processor, 16 GB RAM, and a 256 GB SSD hard disk. The analytical results are fairly accurate in all configurations. Most importantly, in the example [*], the numerical integration approach requires approximately 3 hours, 14 minutes, and 36 seconds, whereas the closed-form expression requires only 0.014 seconds. In the 8-element example in [41], the numerical integration requires 8 hours, 51 minutes, and 22 seconds, while the closed-form expression just 0.0154 seconds. In the example with 16 elements in [42], the numerical integration requires 11 hours, 56 minutes, and 23 seconds, while the closed-form expression only 0.0179 seconds. Hence, it is concluded that using the numerical integration method will not be time effective as the number of elements increases. The absolute accuracy error between the two approaches is less than 0.5% for all configurations, as shown in Table 1. It should be noted that incorporating higher-order harmonics ($|q_s| > 1000$) into the numerical technique further reduces the error rate. However, the calculation time will be significantly longer. As a result,

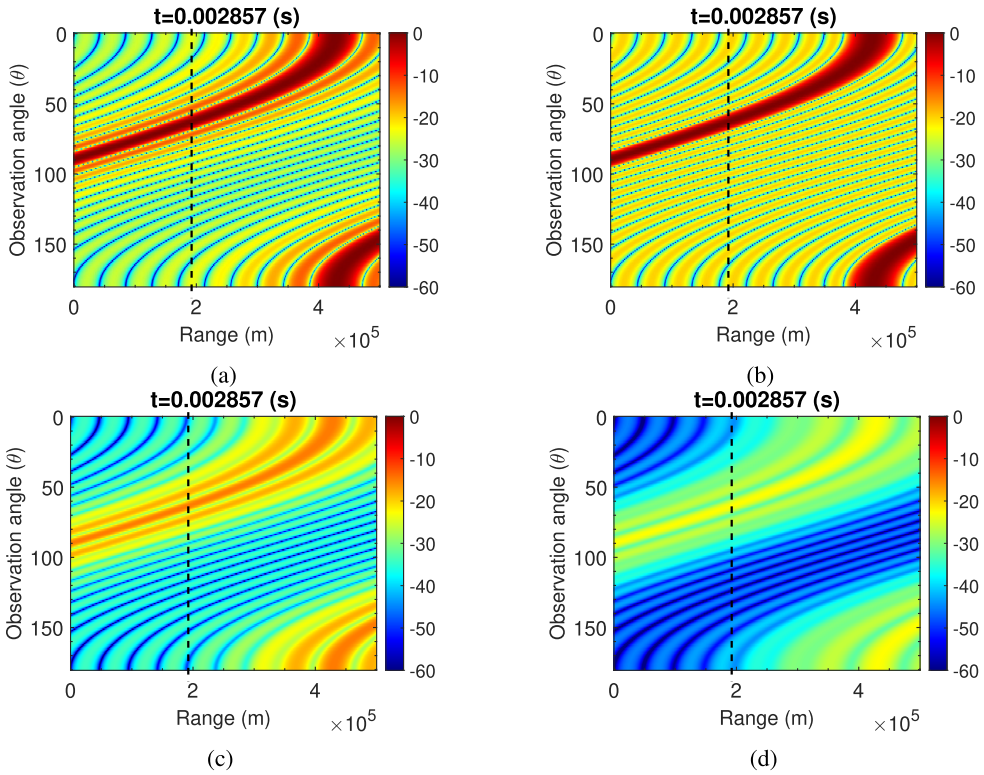

FIGURE 4. The normalized range-angle field distribution for two different pulse duration strategies (a) identical pulse duration $\tau_n = 0.4$ (Example-1), (b) pulse durations are chosen from a Chebshyev distribution for -20 dB SLL (Example-2) at $q = 0$ (c) $q = 1$, (d) $q = 2$.

the proposed closed-form expression is extremely accurate and helpful.

Another interesting finding is that (24) is only dependent on the normalized pulse durations. When compared to the radiated power expressions of conventional array antenna systems [38], [41], this may appear unexpected. In particular, the radiated power is independent of the distance between the elements. However, when the $(N-1)\Delta_f < f_p$ criterion is valid, it is apparent that the array element harmonics will not overlap in the frequency spectrum. Therefore, it can be deduced that the correlation between the harmonic radiations of the array elements at different frequencies will be insignificant.

C. DISCUSSION ON EXPERIMENTAL VERIFICATION

As described in the preceding sections, the range periodicities of pulsed FDA's radiation are typically in the km order and time-dependent. Thus, an area with a radius of at least one range period must be considered in order to conduct an experimental verification. Within such an area, it would take a huge number of receivers to achieve a significant resolution (e.g., about 100m). Furthermore, this architecture should be implemented at a certain height from the ground to minimize the effects of multipath, reflections, and interference from other sources. As a result, the FDA's radiation fields are unlikely to be experimentally validated in such formidable conditions. For this reason, in recent studies on FDA radar applications (e.g., [43], [44]), where range-dependent radiation is thought to provide significant benefits, only numerical results have been demonstrated (rather than experimental ones). Moreover, since the discussions about the FDA's theoretical background (mostly on time dependency) will continue, it is more reasonable to wait until the literature reaches a certain level of knowledge, or until a more practical experimental setup is presented, before proceeding into an experimental verification.

In addition to the case introduced above, measurements must be performed at all instants throughout a period at an infinite number of frequencies resulting from periodic excitations to calculate the SRP, which is extremely challenging experimentally with the existing technological tools. Even in a truncated harmonic model (discussed in Section V-B), multiple harmonics must be observed at the same time instant, necessitating high-frequency equipment, such as wideband antennas, integrated filters, and so on. However, the truncated approach does not produce exact results; to obtain more accurate results, much more harmonics must be taken into consideration experimentally, which is impractical and increases the hardware complexity. For all these reasons, it is concluded that the SRP is still not an experimentally demonstrable quantity, and, hence, all studies on the SRP in the literature have used the numerical verification technique [48].

In addition to the above discussion, a state-of-the-art comparison table is presented to highlight the differences between this study and the TMA, FDA, and pulsed FDA

TABLE 2. A comparative overview: State-of-the-art features in TMAs, FDAs, and pulsed-FDAs.

	TMA			FDA		pulsed-FDA	
Feature	[45]	[46]	[47]	[37]	[11]	[29]	This work
Range Dependency	✗	✗	✗	✓	✓	✓	✓
Prototype	✗	✓	✓	✓	✗	✗	✗
Pattern verification	✗	✓	✗	✗	✗	✗	✗
SRP	✓	✓	✓	✗	✗	✓	✓
SRP verification	Numerical	✗	✗	✗	✗	✗	Numerical

studies already found in the literature. As shown in Table 2, the SRP plays a crucial role in TMA and pulsed-FDA studies, where only switching strategies can be adapted. This issue is not a concern in classical FDAs, where no switching circuit is applied. Additionally, in FDA and pulsed-FDA systems, where modulated versions of the same signal at different frequencies are used, unlike TMAs, range dependency becomes a critical concern. While TMAs have been demonstrated on experimental prototypes that incorporate switches capable of operating at high frequencies and allow 2D pattern measurements, FDAs have experimental prototypes that permit measurements from a single point on the broadside only, making 2D pattern measurements unfeasible. Finally, in TMA and pulsed-FDA systems, where SRP is a common term, only numerical methods are used for verification; as stated earlier, experimental verification is impossible to date.

VI. CONCLUSION

In this paper, a harmonic-based analysis and power calculations of the pulsed FDA structure were carried out. First, a summary of the structure was provided, followed by a focus on harmonic analysis, and it was articulated that radiation occurred as a harmonic-range-angle-dependent process. Furthermore, it was articulated that periodicity-induced radiation in harmonics consumes power and that it would be critical to take this into account during the design phase. Then, the analytical calculation of the power consumed in the harmonics of pulsed FDAs with their already known configuration was carried out and numerically validated. Moreover, the effect of duration on pattern shaping and power consumption was investigated through comparative examples with various configurations. Finally, the limitations of the configurations proposed in the literature to obtain time-independent radiation were discussed in terms of power consumption.

APPENDIX

To derive (22), the integral in (21) should be calculated first as follows [38]:

$$\underset{\substack{q=p\\ m=n}}{\Xi} = \frac{1}{t_p}\int_{t'=0}^{t_p}\sum_{n=0}^{N-1}\cos\left(2\pi(f_0+qf_p+n\Delta_f)\,t'+\varphi_{nq}\right)^2 dt'$$

$$= \frac{1}{2} + \frac{\cos\left(2\pi(b+qh+n)+2\phi_{nq}\right)\sin\left(2\pi\,(b+qh+n)\right)}{4\pi(b+qh+n)}, \tag{29}$$

where $b=\frac{f_0}{\Delta_f}$, $h=\frac{f_p}{\Delta_f}$. It should be noted that the numerator of the second part of (29) is in $[-1,1]$. Additionally, the maximum value of the second part is equal to $\frac{1}{4\pi(b+qh+n)}$. When $\Delta_f \ll f_0$ is chosen, the denominator of this quantity grows large. Under these circumstances, the second part is very close to zero, so it can be neglected.

Similarly, the integration for $m \neq n$ can be expressed as follows:

$$\underset{\substack{q=p\\ m\neq n}}{\Xi} = \frac{1}{t_p}\int_{t'=0}^{t_p}\cos\left(2\pi(f_0+qf_p+n\Delta_f)\,t'+\varphi_{nq}\right) \times\cos\left(2\pi(f_0+qf_p+m\Delta_f)\,t'+\varphi_{mq}\right)dt'. \tag{30}$$

Here, Ξ represents the integral operators of states. Furthermore, with the help of trigonometric identities (30), can be written in two parts as follows:

$$\underset{\substack{q=p\\ m\neq n}}{\Xi} = \frac{1}{2t_p}\int_{t'=0}^{t_p}\cos\left(2\pi(2(f_0+qf_p)+(n+m)\Delta_f)t'+\varphi_{nq}+\varphi_{mq}\right)dt' + \frac{1}{2t_p}\int_{t'=0}^{t_p} cos(2\pi(n-m)\Delta_f)-\varphi_{nq}-\varphi_{mq})dt'. \tag{31}$$

The first part of (31) can be taken as zero if $\Delta_f \ll f_0$ holds. Then, the second part is also calculated as zero for $t_p=\frac{1}{\Delta_f}$. A similar method can be applied for $p \neq q$ state. There is also $m=n$ and $m\neq n$ situation. For $m=n$, the integral is calculated as follows:

$$\underset{\substack{q\neq p\\ m\neq n}}{\Xi} = \frac{1}{t_p}\int_{t'=0}^{t_p}\cos\left(2\pi(f_0+qf_p+n\Delta_f)\,t'+\varphi_{nq}\right) \times\cos\left(2\pi(f_0+pf_p+n\Delta_f)\,t'+\varphi_{np}\right)dt'. \tag{32}$$

With the help of trigonometric identities, (32) can be written as follows:

$$\underset{\substack{q\neq p\\ m=n}}{\Xi} = \frac{1}{2t_p}\int_{t'=0}^{t_p}\cos\left(2\pi(2f_0+(q+p)f_p+2n\Delta_f)\,t'+\varphi_{nq}+\varphi_{np}\right)dt' + \frac{1}{2t_p}\int_{t'=0}^{t_p}\cos\left(2\pi(p-q)f_p\right)t'-\varphi_{nq}-\varphi_{mq})dt'. \tag{33}$$

If $f_0 \gg f_p$, this part can be taken as zero. By following the same methodology for $q \neq p$ and $m \neq n$, under the same conditions such as $f_0 \gg f_p$, $\Delta_f \ll f_p$, this part can be also negligible. As a result, the power is just radiated at the $p = q$ and $m = n$ states.

REFERENCES

[1] R. J. Mailloux, "Phased array theory and technology," *Proc. IEEE*, vol. 70, no. 3, pp. 246–291, Mar. 1982.

[2] P. Antonik, M. C. Wicks, H. D. Griffiths, and C. J. Baker, "Frequency diverse array radars," in *Proc. IEEE Conf. Radar*, Apr. 2006, p. 3.

[3] D. Cohen, D. Cohen, and Y. C. Eldar, "High resolution FDMA MIMO radar," *IEEE Trans. Aerosp. Electron. Syst.*, vol. 56, no. 4, pp. 2806–2822, Aug. 2020.

[4] J. Farooq, M. A. Temple, and M. A. Saville, "Exploiting frequency diverse array processing to improve SAR image resolution," in *Proc. IEEE Radar Conf.*, May 2008, pp. 1–5.

[5] J. Xu, G. Liao, S. Zhu, and H. C. So, "Deceptive jamming suppression with frequency diverse MIMO radar," *Signal Process.*, vol. 113, pp. 9–17, Aug. 2015.

[6] J. Xu, S. Zhu, and G. Liao, "Range ambiguous clutter suppression for airborne FDA-STAP radar," *IEEE J. Sel. Topics Signal Process.*, vol. 9, no. 8, pp. 1620–1631, Dec. 2015.

[7] P. Antonik, M. C. Wicks, H. D. Griffiths, and C. J. Baker, "Multi-mission multi-mode waveform diversity," in *Proc. IEEE Conf. Radar*, Apr. 2006, p. 3.

[8] Ç. Cagri, "Analysis of frequency diverse arrays for radar and communication applications," Ph.D. dissertation, Dept. Elect. Electron. Eng., Middile East Tech. Univ., Turkey, Nov. 2015.

[9] A. Aytun, "Frequency diverse array radar," Ph.D. dissertation, Nav. Postgraduate School, Monterey, CA, USA, 2010.

[10] W.-Q. Wang, "Range-angle dependent transmit beampattern synthesis for linear frequency diverse arrays," *IEEE Trans. Antennas Propag.*, vol. 61, no. 8, pp. 4073–4081, Aug. 2013.

[11] A. Akkoc, N. A. Korkmaz, Y. Genc, E. Afacan, and E. Yazgan, "Time-invariant and localized secure reception with sequential multi-carrier receive-FDA," *IEEE Trans. Antennas Propag.*, vol. 71, no. 9, pp. 7064–7072, Sep. 2023.

[12] W.-Q. Wang, H. C. So, and H. Shao, "Nonuniform frequency diverse array for range-angle imaging of targets," *IEEE Sensors J.*, vol. 14, no. 8, pp. 2469–2476, Aug. 2014.

[13] Y. Liao, W.-Q. Wang, and Z. Zheng, "Frequency diverse array beampattern synthesis using symmetrical logarithmic frequency offsets for target indication," *IEEE Trans. Antennas Propag.*, vol. 67, no. 5, pp. 3505–3509, May 2019.

[14] M. Tan, C. Wang, B. Xue, and J. Xu, "A novel deceptive jamming approach against frequency diverse array radar," *IEEE Sensors J.*, vol. 21, no. 6, pp. 8323–8332, Mar. 2021.

[15] A. Akkoc, E. Afacan, and E. Yazgan, "Dot-shaped 3D range-angle dependent beamforming with discular frequency diverse array," *IEEE Trans. Antennas Propag.*, vol. 69, no. 10, pp. 6500–6508, Oct. 2021.

[16] W. Khan, I. M. Qureshi, and S. Saeed, "Frequency diverse array radar with logarithmically increasing frequency offset," *IEEE Antennas Wireless Propag. Lett.*, vol. 14, pp. 499–502, 2015.

[17] M. Tan, C. Wang, Z. Li, J. Bai, and L. Bao, "Adaptive beamforming using frequency diverse MIMO radar with nonlinear frequency offset," in *Proc. IEEE 11th Sensor Array Multichannel Signal Process. Workshop (SAM)*, Jun. 2020, pp. 1–5.

[18] H. Shao, J. Dai, J. Xiong, H. Chen, and W.-Q. Wang, "Dot-shaped range-angle beampattern synthesis for frequency diverse array," *IEEE Antennas Wireless Propag. Lett.*, vol. 15, pp. 1703–1706, 2016.

[19] J. Xiong, W.-Q. Wang, H. Shao, and H. Chen, "Frequency diverse array transmit beampattern optimization with genetic algorithm," *IEEE Antennas Wireless Propag. Lett.*, vol. 16, pp. 469–472, 2017.

[20] Y. Ding, A. Narbudowicz, and G. Goussetis, "Physical limitation of range-domain secrecy using frequency diverse arrays," *IEEE Access*, vol. 8, pp. 63302–63309, 2020.

[21] M. Secmen, S. Demir, A. Hizal, and T. Eker, "Frequency diverse array antenna with periodic time modulated pattern in range and angle," in *Proc. IEEE Radar Conf.*, Apr. 2007, pp. 427–430.

[22] Q. Cheng, J. Zhu, T. Xie, J. Luo, and Z. Xu, "Time-invariant angle-range dependent directional modulation based on time-modulated frequency diverse arrays," *IEEE Access*, vol. 5, pp. 26279–26290, 2017.

[23] C. Cui, W. Li, and X. Shi, "Quasi-time-invariant range-angle-decoupled beampattern synthesis of frequency diverse arrays," in *Proc. Int. Conf. Microw. Millim. Wave Technol. (ICMMT)*, May 2019, pp. 1–3.

[24] A.-M. Yao, W. Wu, and D.-G. Fang, "Frequency diverse array antenna using time-modulated optimized frequency offset to obtain time-invariant spatial fine focusing beampattern," *IEEE Trans. Antennas Propag.*, vol. 64, no. 10, pp. 4434–4446, Oct. 2016.

[25] W. Khan and I. M. Qureshi, "Frequency diverse array radar with time-dependent frequency offset," *IEEE Antennas Wireless Propag. Lett.*, vol. 13, pp. 758–761, 2014.

[26] M. Zubair, S. Ahmed, and M.-S. Alouini, "Frequency diverse array radar: A closed-form solution to design weights for desired beampattern," in *Proc. IEEE Int. Conf. Acoust., Speech Signal Process. (ICASSP)*, May 2020, pp. 4687–4691.

[27] K. Chen, S. Yang, Y. Chen, and S.-W. Qu, "Accurate models of time-invariant beampatterns for frequency diverse arrays," *IEEE Trans. Antennas Propag.*, vol. 67, no. 5, pp. 3022–3029, May 2019.

[28] M. Tan, C. Wang, and Z. Li, "Correction analysis of frequency diverse array radar about time," *IEEE Trans. Antennas Propag.*, vol. 69, no. 2, pp. 834–847, Feb. 2021.

[29] Y. Xu, X. Shi, J. Xu, and P. Li, "Range-angle-dependent beamforming of pulsed frequency diverse array," *IEEE Trans. Antennas Propag.*, vol. 63, no. 7, pp. 3262–3267, Jul. 2015.

[30] W. T. Li, Y. Q. Hei, X. W. Shi, and H. C. So, "Range-angle-dependent beamforming with FDA using four-dimensional arrays," *Signal Process.*, vol. 147, pp. 68–79, Jun. 2018.

[31] T. Tiberi, E. Fazzini, A. Costanzo, and D. Masotti, "Exploitation of harmonic generation in time-controlled frequency diverse arrays for WPT," *IEEE Trans. Antennas Propag.*, doi: 10.1109/TAP.2023.3324499.

[32] C. Cui, W. Li, X. Ye, Y. Hei, and X. Shi, "A short-time range-angle-decoupled beam pattern synthesis for frequency diverse arrays," *IET Microw., Antennas Propag.*, vol. 15, no. 8, pp. 855–870, Mar. 2021.

[33] W.-Q. Wang, H. C. So, and A. Farina, "An overview on time/frequency modulated array processing," *IEEE J. Sel. Topics Signal Process.*, vol. 11, no. 2, pp. 228–246, Mar. 2017.

[34] Y. Liao, G. Zeng, Z. Luo, and Q. H. Liu, "Time-variance analysis for frequency-diverse array beampatterns," *IEEE Trans. Antennas Propag.*, vol. 71, no. 8, pp. 6558–6567, Aug. 2023.

[35] S. Y. Nusenu and A. Basit, "Frequency diverse array antennas: From their origin to their application in wireless communication systems," *J. Comput. Netw. Commun.*, vol. 2018, pp. 1–12, Apr. 2018.

[36] T. Tiberi, E. Fazzini, A. Costanzo, and D. Masotti, "Realistic performance analysis of frequency-diverse arrays radiation," in *Proc. IEEE 13th Int. Conf. RFID Technol. Appl. (RFID-TA)*, Sep. 2023, pp. 217–220.

[37] T. Eker, S. Demir, and A. Hizal, "Exploitation of linear frequency modulated continuous waveform (LFMCW) for frequency diverse arrays," *IEEE Trans. Antennas Propag.*, vol. 61, no. 7, pp. 3546–3553, Jul. 2013.

[38] J. C. Bregains, J. Fondevila-Gomez, G. Franceschetti, and F. Ares, "Signal radiation and power losses of time-modulated arrays," *IEEE Trans. Antennas Propag.*, vol. 56, no. 6, pp. 1799–1804, Jun. 2008.

[39] E. Aksoy and E. Afacan, "Thinned nonuniform amplitude time-modulated linear arrays," *IEEE Antennas Wireless Propag. Lett.*, vol. 9, pp. 514–517, 2010.

[40] E. Aksoy, "Calculation of sideband radiations in time-modulated volumetric arrays and generalization of the power equation," *IEEE Trans. Antennas Propag.*, vol. 62, no. 9, pp. 4856–4860, Sep. 2014.

[41] I. Kanbaz, U. Yesilyurt, S. Kuzu, and E. Aksoy, "Total harmonic power of arbitrarily switched nonuniform period time-modulated arrays," *IEEE Antennas Wireless Propag. Lett.*, vol. 19, no. 1, pp. 193–197, Jan. 2020.

[42] I. Kanbaz, U. Yesilyurt, and E. Aksoy, "A new approach for harmonic power calculation of nonuniform time modulated arrays," in *Proc. Int. Symp. Fundam. Electr. Eng. (ISFEE)*, Nov. 2018, pp. 1–4.

[43] W. Lv, K. V. Mishra, and S. Chen, "Co-pulsing FDA radar," *IEEE Trans. Aerosp. Electron. Syst.*, vol. 59, no. 2, pp. 1107–1126, Apr. 2023.

[44] P. Gong, Z. Zhang, Y. Wu, and W.-Q. Wang, "Joint design of transmit waveform and receive beamforming for LPI FDA-MIMO radar," *IEEE Signal Process. Lett.*, vol. 29, pp. 1938–1942, 2022.

[45] S. Mandal and S. K. Mandal, "Efficient computation of sideband power losses in pulse-shifted non-uniform time-modulated array with arbitrary element pattern," *Prog. Electromagn. Res. B*, vol. 98, pp. 59–75, 2023.

[46] J. Guo, S. Yang, Y. Chen, P. Rocca, J. Hu, and A. Massa, "Efficient sideband suppression in 4-D antenna arrays through multiple time modulation frequencies," *IEEE Trans. Antennas Propag.*, vol. 65, no. 12, pp. 7063–7072, Dec. 2017.
[47] Y. Gao, X. Liang, L. Xiang, J. Chen, C. He, J. Geng, and R. Jin, "Analysis and design of high-efficiency single-sideband time-modulated module," *IEEE Trans. Microw. Theory Techn.*, doi: 10.1109/TMTT.2023.3289226.
[48] Q. Zeng, P. Yang, L. Yin, H. Lin, C. Wu, F. Yang, and S. Yang, "Calculation of the total radiated power for 4-D antenna arrays with arbitrary time modulated waveform," *IEEE Trans. Antennas Propag.*, vol. 69, no. 12, pp. 9015–9020, Dec. 2021.

IHSAN KANBAZ (Member, IEEE) was born in Sanliurfa, Turkey, in 1991. He received the M.Sc. degree in electrical and electronics engineering from Mersin University, Mersin, Turkey, in 2018, and the Ph.D. degree in electrical and electronics engineering from Gazi University, Ankara, Turkey. He is currently a Research Assistant with Gazi University and did his postdoctoral research with Queen's University Belfast. His research interests include antenna design, test and measurement, adaptive arrays, optimization, and metaheuristic algorithms.

UGUR YESILYURT (Member, IEEE) was born in Erzurum, Turkey, in 1990. He received the bachelor's degree from the Department of Electrical and Electronics Engineering, Atatürk University, Erzurum, in 2013, and the M.Sc. and Ph.D. degrees in electrical and electronics engineering from Gazi University, Ankara, Turkey, in 2018 and 2023, respectively. He is currently an Assistant Professor with Erzurum Technical University. His research interests include antenna radiation patterns, time-modulated antenna arrays, frequency diverse arrays, and antenna design.

GALIP ORKUN ARICAN (Member, IEEE) received the B.S. degree from Bilkent University, in 2010, the M.S. degree from Middle East Technical University, in 2014, and the Ph.D. degree from Gazi University, in 2021. From 2010 to 2015, he was a MMIC Design Engineer with the Nanotechnology Research Center, Bilkent University. Since 2015, he has been a RF/Microwave Design Engineer with ASELSAN Inc. His research interests include high frequency applications, GaN/GaAs MMICs, hybrid modules, satellite communication, microstrip antennas, filters, and electromagnetic theory.

ERTUGRUL AKSOY (Member, IEEE) received the M.Sc. and Ph.D. degrees in electrical and electronics engineering from Gazi University, Ankara, Turkey, in 2008 and 2012, respectively. He has been an Associate Professor with Gazi University, since 2017. He has authored or coauthored over 60 peer-reviewed scientific articles on antenna arrays and optimization field. His current research interests include antenna engineering, computational electromagnetics, evolutionary optimization, temporal arrays, and meta- and frequency-selective structures in electromagnetic engineering. He is a member of the IEEE Antennas and Propagation Society and the IEEE Computational Intelligence Society. He has served as a reviewer for many journals and a TPC member for many international conferences.

MICHAIL MATTHAIOU (Fellow, IEEE) was born in Thessaloniki, Greece, in 1981. He received the Diploma degree in electrical and computer engineering from the Aristotle University of Thessaloniki, Greece, in 2004, the M.Sc. degree (Hons.) in communication systems and signal processing from the University of Bristol, U.K., in 2005, and the Ph.D. degree from the University of Edinburgh, U.K., in 2008.

From September 2008 to May 2010, he was with the Institute for Circuit Theory and Signal Processing, Munich University of Technology (TUM), Germany, as a Postdoctoral Research Associate. He is currently a Professor in communications engineering and signal processing and the Deputy Director of the Centre for Wireless Innovation (CWI), Queen's University Belfast, U.K., after holding an assistant professor position with the Chalmers University of Technology, Sweden. His research interests include signal processing for wireless communications, beyond massive MIMO, intelligent reflecting surfaces, mm-wave/THz systems, and deep learning for communications. He and his coauthors received the IEEE Communications Society (ComSoc) Leonard G. Abraham Prize, in 2017. He also holds the ERC Consolidator Grant BEATRICE (2021–2026) focused on the interface between information and electromagnetic theories. To date, he has received the prestigious 2023 Argo Network Innovation Award, the 2019 EURASIP Early Career Award, and the 2018/2019 Royal Academy of Engineering/The Leverhulme Trust Senior Research Fellowship. His team was also the Grand Winner of the 2019 Mobile World Congress Challenge. He was a recipient of the 2011 IEEE ComSoc Best Young Researcher Award for the Europe, Middle East and Africa Region, and a co-recipient of the 2006 IEEE Communications Chapter Project Prize for the best M.Sc. dissertation in the area of communications. He has coauthored papers that received Best Paper Awards at the 2018 IEEE WCSP and 2014 IEEE ICC. In 2014, he received the Research Fund for International Young Scientists from the National Natural Science Foundation of China. He is currently the Editor-in-Chief of *Physical Communication* (Elsevier), a Senior Editor of IEEE Wireless Communications Letters and *IEEE Signal Processing Magazine*, and an Associate Editor of IEEE Transactions on Communications.